Research Article

INS/WSN-Integrated Navigation Utilizing LS-SVM and H_∞ Filtering

Yuan Xu,[1,2] Xiyuan Chen,[1,2] and Qinghua Li[1,3]

[1] *School of Instrument Science and Engineering, Southeast University, Nanjing 210096, China*
[2] *Key Laboratory of Micro-Inertial Instrument and Advanced Navigation Technology, Ministry of Education, Nanjing 210096, China*
[3] *School of Electrical Engineering and Automation, Shandong Polytechnic University, Jinan 250353, China*

Correspondence should be addressed to Xiyuan Chen, xy_abric@126.com

In order to achieve continuous navigation capability in areas such as tunnels, urban canyons, and indoors a new approach using least squares support vector machine (LS-SVM) and H_∞ filter (HF) for integration of INS/WSN is proposed. In the integrated system, HF estimates the errors of position and velocity while the signals in WSNs are available. Meanwhile, the compensation model is trained by LS-SVM with corresponding HF states. Once outages of the signals in WSNs, the model is used to correct INS solution as HF does. Moreover, due to device reasons, there are slight fluctuations in sampling period in practice. For overcoming this problem of integrated navigation, the theoretical analysis and implementation of HF for an integrated navigation system with stochastic uncertainty are also given. Simulation shows the performance of HF is more robust compared with INS-only solution and Kalman filter (KF) solution, and the prediction of LS-SVM has the smallest error compared with INS-only and back propagation (BP), the improvement is particularly obvious.

1. Introduction

The demand for location-based services (LBSs) has been driving the need for the accurate positioning techniques in the past and is expected to remain the same in the future [1, 2]. Wireless sensor network (WSN) has boomed in the last decades, it shows great potential to develop positioning system in the environments such as tunnels, urban canyons, and indoors, where the Global Positioning Systems (GPS) cannot provide a solution with consistent and long-term stable accuracy due to satellite signal blockage [3–7]. So, the physical location becomes one of key applications in WSNs recently. Most of the current wireless localization in WSN employs the measurement of one or several physical parameters of the radio signal

transmitted between the reference nodes (RNs) and blind nodes (BNs) [8]. For example, Patwari et al. employed the measurements of time of arrival (TOA) and received signal strength (RSS) to estimate relative location in WSNs in 2003 [9]. In 2002, Al-Jazzar and Caffery Jr. estimated node location for nonline of sight (NLOS) environments by TOA [10], then Al-Jazzar et al. used a joint TOA/AOA (so-called angle of arrival) constrained minimization method for locating wireless devices in nonline-of-sight environment in 2009 [11]. Alsindi et al. employed TOA for ranging in indoor multipath environments in 2009 [12]. The mainstream method is to use electromagnetic waves for indoor localization, but due to the high propagation speed, the accuracy is of the order of several meters. On the other hand, some researchers employ ultrasonic waves to achieve high accuracy with narrow bandwidth and narrow directional characteristics, for example, a fully distributed localization system based on ultrasound is proposed by Minami et al., and the accuracy of localization is about 20 cm with 24 devices [13]. Although WSN is capable of indoor wireless localization with the characteristics of low power, low cost, and low complexity, it requires high density of RNs for high accuracy due to its short-distance communication. Therefore, it has to employ a large number of RNs to keep localization accuracy if localization area is large.

Differing from WSN-based wireless localization requiring RNs, INS is a self-contained system incorporating three orthogonal accelerometers and two orthogonal gyroscopes [1]. It is capable of providing positioning information independently. However, for the INS accuracy deteriorates with time due to possible inherent sensor errors (white noise, correlated random noise, bias instability, and angle random walk) that exhibit considerable long-term growth [14–17], it is just a short-term compensation to GPS outages, and the INS cannot maintain long-term high accuracy when GPS signals are unavailable. Thus, INS is poor in long-term self-contained navigation.

Aiming at continuous navigation capability, many intelligent integration navigation approaches have been employed. For instance, Kim et al. presented an integrated GPS/INS/Vision system for helicopter navigation [18], Berefelt et al. used GPS/INS navigation in urban environment [19]. In this mode, training the compensation model by Artificial Intelligence (AI) techniques is widely used to improve the performance of integrated navigation, especially the neural network (NN), as in, for example, the use of the NN for denoising inertial outputs based on microelectromechanical system (MEMS) in [20], and the NN for the compensation model in [21]. However, to achieve good performance it has to select sufficient data samples of good quality for the NN [22], and it is poor in high dimension input spaces. Current algorithms for good quality samples of the compensation model are mainly based on integration filter, as the core of an integrated system, the integration filter should be carefully designed. The KF is one of the most common examples for filtering. With the stochastic state space model of the system and measurement outputs, it is able to achieve the optimal estimation of states in multi-input, multioutput (MIMO) systems [23]. However, due to the noises of system and measurement should be corrupted by white noise and the state estimation is approached with the minimization of the covariance of the estimation error, the KF is not suitable for nonlinear systems. Through the first-order linearization of the nonlinear system, extended KF (EKF) is able to achieve nonlinear estimation. However, for the state distribution is assumed as a Gaussian random variable (GRV), it may generate large errors in the true posterior mean and covariance of the transformed GRV, which can lead to suboptimal performance and sometimes divergence of the filter [24]. Moreover, the system with GRV is often unavailable in practice.

In this paper, we present INS/WSN integration using LS-SVM and HF for long-distance continuous navigation in areas such as tunnels, urban canyons, and indoors. Aiming at the robust performance of filtering, the HF is employed to estimate errors of position and velocity while signals in WSNs are available. Meanwhile, compensation model is trained by LS-SVM, which is used to correct the INS errors during signals in WSN outages. Simulation is employed to evaluate the performance of the proposed method. The results of filtering are compared with the INS-only solution and KF solution, moreover, the results of prediction are compared with the INS-only method and BP method. The remainder of the paper is organized as follows: HF for integration and LS-SVM model are described in Section 2 and Section 3, respectively. Section 4 gives the hybrid method for INS/WSN integration. Simulations and the analyses of experiment results based on semiphysical can be obtained in detail in Section 5. Finally, the conclusions are given.

For convenience, this paper adopts the following notations.

A': transpose of a matrix or vector A.

$A > 0$ ($A \geq 0$): A is positive definite (positive semidefinite) symmetric matrix.

S_n: the set of all real symmetric matrices.

R^n: n-dimensional Euclidean space.

$I_{n \times n}$: $n \times n$ identity matrix.

2. H_∞ Fusion Filter for Integration

2.1. Stochastic Uncertain System

In order to achieve robust performance, HF is widely analyzed and used in the nonlinear systems [25–27]. The HF is to design an estimator to estimate the unknown state combination with measurement output [28]. In contrast with the KF and EKF, one of the main advantages of HF is that it is not necessary to know exactly the statistical properties of the noise but only on the assumption of the noise with bounded energy [29], which makes this technique useful in certain practical applications. For the above-mentioned reasons, HF technique has been extensively developed in the last decade, and many HF-based methods have been proposed, especially in the field of stochastic systems. For instance, Xu and Chen proposed an H_∞ filtering for uncertain impulsive stochastic systems under sampled measurements in [30]. Zhang and Chen studied the exact observability of stochastic systems in [29], and, then, they solved the problem of filtering for nonlinear stochastic uncertain system [28].

As WSN-based wireless localization is a relative localization, HF uses relative errors of position and velocity of BN as the state vector. Ideally, the relative position errors of BN measured by INS at k state are able to be illustrated in (2.1):

$$e_{x,k+1} = e_{x,k} + T \cdot e_{vx,k} + \omega_{x,k},$$

$$e_{y,k+1} = e_{y,k} + T \cdot e_{vy,k} + \omega_{y,k},$$

(2.1)

where (e_x, e_y) is the relative position error of BN at k moment, (e_{vx}, e_{vy}) is the velocity error of BN at k moment, and T is ideal sample time. Due to the limitation of timing device, there

will be a stochastic error for ideal sample time in practice. It leads the system in (2.1) to be a stochastic uncertain system, which is expressed as follow:

$$e_{x,k+1} = e_{x,k} + \left((T + \delta t) \cdot \beta_k\right) \cdot e_{vx,k} + \omega_{x,k},$$
$$e_{y,k+1} = e_{y,k} + \left((T + \delta t) \cdot \beta_k\right) \cdot e_{vy,k} + \omega_{y,k}. \tag{2.2}$$

Here δt is the stochastic uncertainty of system and β_k is a standard random scalar sequences with zero mean. Thus, the model of the system in (2.2) can be written in matrix form:

$$\begin{bmatrix} e_{x,k+1} \\ e_{y,k+1} \\ e_{vx,k+1} \\ e_{vy,k+1} \end{bmatrix} = \left\{ \begin{bmatrix} 1 & 0 & T & 0 \\ 0 & 1 & 0 & T \\ 0 & 0 & 1 & 0 \\ 0 & 0 & 0 & 1 \end{bmatrix} + \begin{bmatrix} 0 & 0 & \delta t & 0 \\ 0 & 0 & 0 & \delta t \\ 0 & 0 & 0 & 0 \\ 0 & 0 & 0 & 0 \end{bmatrix} \beta_k \right\} \begin{bmatrix} e_{x,k} \\ e_{y,k} \\ e_{vx,k} \\ e_{vy,k} \end{bmatrix} + \begin{bmatrix} \omega_{x,k} \\ \omega_{y,k} \\ \omega_{vx,k} \\ \omega_{vy,k} \end{bmatrix}. \tag{2.3}$$

Here, we denote (2.3) as (2.4).

$$X_{k+1} = \left(A + E \cdot \beta_k\right) X_k + B\omega_k, \tag{2.4}$$

where $\omega_k \in R^m$ is stochastic process noise which belongs to $l_2[0,\infty)$.

The observation vectors of the HF are formed by differencing the INS and WSN positions $(r_{\text{WSN}}, r_{\text{INS}})$ and the velocities $(v_{\text{WSN}}, v_{\text{INS}})$. Thus, the observation equation is illustrated as (2.5):

$$\begin{bmatrix} \Delta r_{x,k} \\ \Delta r_{y,k} \\ \Delta v_{x,k} \\ \Delta v_{y,k} \end{bmatrix} = \begin{bmatrix} 1 & 0 & 0 & 0 \\ 0 & 1 & 0 & 0 \\ 0 & 0 & 1 & 0 \\ 0 & 0 & 0 & 1 \end{bmatrix} \begin{bmatrix} e_{x,k} \\ e_{y,k} \\ e_{vx,k} \\ e_{vy,k} \end{bmatrix} + \begin{bmatrix} v_{x,k} \\ v_{y,k} \\ v_{vx,k} \\ v_{vy,k} \end{bmatrix}, \tag{2.5}$$

where $\Delta r_{x,k} = r_{x,k(\text{INS})} - r_{x,k(\text{WSN})}$, $\Delta r_{y,k} = r_{y,k(\text{INS})} - r_{y,k(\text{WSN})}$, $\Delta v_{x,k} = v_{x,k(\text{INS})} - v_{x,k(\text{WSN})}$, and $\Delta v_{y,k} = v_{y,k(\text{INS})} - v_{y,k(\text{WSN})}$.

Here, we denote (2.5) as (2.6).

$$Y_k = CX_k + Dv_k, \tag{2.6}$$

where $v_k \in R^m$ is measurement noise which belongs to $l_2[0,\infty)$. For the convenience, we assume that

$$E\sum_{k=0}^{\infty} \omega'_k \omega_k < \infty, \qquad E\sum_{k=0}^{\infty} v'_k v_k < \infty. \tag{2.7}$$

So, the stochastic uncertain system can be simply expressed as:

$$X_{k+1} = (A + E \cdot \beta_k)X_k + B_1\varsigma_k,$$

$$Y_k = CX_k + D_1\varsigma_k, \tag{2.8}$$

$$Z_k = LX_k.$$

Here, Z_k is the state combination to be estimated, $B_1 = [B\ 0]$, $D_1 = [0\ D]$, and $\varsigma_k = [\omega'_k\ \upsilon'_k]'$.

2.2. H_∞ Filter Formulation

In this section, we investigate the design of a linear estimator for Z_k of the following form:

$$\widehat{X}_{k+1} = A_f\widehat{X}_k + B_fY_k,$$

$$\widehat{Z}_k = L\widehat{X}_k, \quad k = 0, 1, 2, \ldots, \tag{2.9}$$

where $\widehat{X}_k$ and $\widehat{Z}_k$ are the estimates of X_k and Z_k, respectively, and $\{A_f, B_f, L\}$ are the constant matrices. Here, we define state error vector and measurement error vector, respectively, as follows:

$$e_k = X_k - \widehat{X}_k, \widetilde{Z}_k = Z_k - \widehat{Z}_k. \tag{2.10}$$

Let $\Xi = E\beta_k$ and $A_f = A - B_fC + \Xi$, then we can obtain the following equation with (2.8), (2.9), and (2.10):

$$e_{k+1} = \left(\widetilde{A} + E\beta_k\right)e_k + \widetilde{B}\varsigma_k,$$

$$\widetilde{Z}_k = Le_k, \tag{2.11}$$

where $\widetilde{A} = A - B_fC$ and $\widetilde{B} = B_1 - B_fD_1$.

For a given scalar $\gamma > 0$, the performance index is illustrated as (2.12):

$$J = E\sum_{k=0}^{\infty}\left(\widetilde{Z}'_k\widetilde{Z}_k - \gamma^2\varsigma'_k\varsigma_k\right). \tag{2.12}$$

In this paper, we look for an H_∞ filter satisfies that for all nonzero ω_k and υ_k with the initial state $X_k = 0$, $J < 0$, and the system (2.11) is asymptotically stable.

2.3. Asymptotic Stability

For future convenience, we give the following lemmas which are very useful for the proof of our main theorem.

Lemma 2.1 (see [31]).

$$X_{k+1} = (A + E\beta_k)X_k + B\varsigma_k,$$
$$Z_k = LX_k,$$

(2.13)

for any $\gamma > 0$, the system (2.13) is asymptotically stable and J in (2.12) is negative for all nonzero $\varsigma_k \in l_2[0, \infty)$ if there exists $P = P' > 0$ that satisfies the inequality

$$-P + A'PA + A'PB\Theta^{-1}B'PA + L'L + E'PE < 0,$$

(2.14)

and also satisfies $\Theta > 0$, where $\Theta = \gamma^2 I - B'PB$.

Lemma 2.2 (Schur's complement). *For real matrices N, $M = M'$, $R = R' < 0$, the following two conditions are equivalent:*

(1) $M - NR^{-1}N' < 0$,

(2) $\begin{bmatrix} M & N \\ N' & R \end{bmatrix} < 0$.

Consider the system of (2.11). We arrive at the following result.

Theorem 2.3. *The condition for system of (2.11) to be asymptotically stable and γ of (2.12) to be existed is that there exists $P = P' > 0$ and Q satisfies the inequality (2.15):*

$$\begin{bmatrix} -P & 0 & A'P - C'Q' & A'P - C'Q' & L' & E'P \\ 0 & -\gamma^2 I & B_1'P - D_1'Q' & 0 & 0 & 0 \\ PA - QC & PB_1 - QD_1 & -P & 0 & 0 & 0 \\ PA - QC & 0 & 0 & -P & 0 & 0 \\ L & 0 & 0 & 0 & -I & 0 \\ PE & 0 & 0 & 0 & 0 & -P \end{bmatrix} < 0.$$

(2.15)

Proof. Consider the system of (2.11) and apply Lemma 2.1, given $\gamma > 0$, a necessary and sufficient condition for J in (2.12) to be negative for all nonzero $\varsigma_k \in l_2[0, \infty)$ which is that there exists $P = P' > 0$ to

$$-P + \tilde{A}'P\tilde{A} + \tilde{A}'P\tilde{B}\tilde{\Theta}^{-1}\tilde{B}'P\tilde{A} + L'L + E'PE < 0,$$

(2.16)

where $\tilde{\Theta} = \gamma^2 I - \tilde{B}'P\tilde{B}$, $P > 0$, and $\tilde{\Theta} > 0$.

Defining $\Delta = -P + \tilde{A}'P\tilde{A} + L'L + E'PE$, so

$$\Delta + \tilde{A}'P\tilde{B}\tilde{\Theta}^{-1}\tilde{B}'P\tilde{A} < 0.$$

(2.17)

Applying Schur's complement, inequality (2.17) and the following inequality are equivalent:

$$\begin{bmatrix} \Delta & \tilde{A}'P\tilde{B} \\ \tilde{B}'P\tilde{A} & -\left(\gamma^2 I - \tilde{B}'P\tilde{B}\right) \end{bmatrix} < 0. \tag{2.18}$$

And inequality (2.18) can be rewritten as inequality (2.19):

$$\begin{bmatrix} \Delta & 0 \\ 0 & -\gamma^2 I \end{bmatrix} - \begin{bmatrix} \tilde{A}' \\ \tilde{B}' \end{bmatrix} P(-P)^{-1} P \begin{bmatrix} \tilde{A} & \tilde{B} \end{bmatrix} < 0. \tag{2.19}$$

Using Schur's complement again, inequality (2.19) is able to be written as (2.20):

$$\begin{bmatrix} \Delta & 0 & \tilde{A}'P \\ 0 & -\gamma^2 I & \tilde{B}'P \\ P\tilde{A} & P\tilde{B} & -P \end{bmatrix} < 0. \tag{2.20}$$

Then, by Lemma 2.1 and $\Delta = -P + \tilde{A}'P\tilde{A} + L'L + E'PE$, we can obtain inequality (2.21) readily:

$$\begin{bmatrix} -P & 0 & \tilde{A}'P & \tilde{A}'P & L' & E'P \\ 0 & -\gamma^2 I & \tilde{B}'P & 0 & 0 & 0 \\ P\tilde{A} & P\tilde{B} & -P & 0 & 0 & 0 \\ P\tilde{A} & 0 & 0 & -P & 0 & 0 \\ L & 0 & 0 & 0 & -I & 0 \\ PE & 0 & 0 & 0 & 0 & -P \end{bmatrix} < 0. \tag{2.21}$$

Now, we substitute (2.11) into inequality (2.21) and define that $Q = PB_f$, then we can obtain inequality (2.15) readily.

Moreover, the matrix inequality is able to be written as following if we set $\gamma^2 = \bar{\gamma}$:

$$\psi(P, Q, \bar{\gamma}) < 0. \tag{2.22}$$

Thus, the solving of the filter is transformed to the following optimisation problem:

$$\min_{p_1 > 0, Q} \bar{\gamma}, \tag{2.23}$$

$$\text{subject to} \quad \text{LMIs(2.22)}.$$

So, the filter is asymptotically stable and there exists the minimum performance index $\sqrt{\gamma}$, the parameters of the HF can obtain by (2.23):

$$B_f = P^{-1}Q, \qquad A_f = A - P^{-1}QC + \Xi. \tag{2.24}$$

For the mean value of Ξ is zero, the A_f is also able to denote as follows:

$$A_f = A - P^{-1}QC. \tag{2.25}$$

$\square$

3. LS-SVM Model and Training Algorithm

LS-SVM is powerful to estimate for nonlinear. It is also able to extract the optimal solution with small training data. The LS-SVM algorithm is employed here to improve the accuracy of the INS-only solution during WSN outages.

3.1. LS-SVM Regression Algorithm

Equation (3.1) shows the optimal linear regression function which is built in feature space. Where b is the bias term and ω is weight vector. Given a training set $\{x_k, y_k\}_{k=1}^n$, the LS-SVM algorithm maps a higher dimensional feature space $\psi(x) = \{\phi(x_1), \phi(x_2), \dots, \phi(x_n)\}$ with nonlinear function $\varphi(x)$:

$$f(x) = \{\omega, \phi(x)\} + b = \sum_{i=1}^N \omega_i \varphi_i(x) + b. \tag{3.1}$$

The optimisation problem is

$$\min_{\omega, b, e} J(\omega, e) = \frac{1}{2}\omega^T \omega + \eta \frac{1}{2}\sum_{k=1}^N e_k^2, \tag{3.2}$$

due to the equality constraints

$$y_k = \omega^T \varphi(x_k) + b + e_k, \quad k = 1, \dots, N. \tag{3.3}$$

To solve the optimisation problem abovementioned, the Lagrangian function is introduced:

$$L(\omega, b, e, \alpha_i) = J(\omega, e) - \sum_{i=1}^N \alpha_i \omega^T \phi(x_i) + b + e_i - y_i, \tag{3.4}$$

where α_i are the Lagrange multipliers, according to Karush Kuhn Tucker (KKT) optimization conditions which are illustrated in (3.5):

$$\frac{\partial L}{\partial \omega} = 0, \qquad \frac{\partial L}{\partial b} = 0, \qquad \frac{\partial L}{\partial e_i} = 0, \qquad \frac{\partial L}{\partial \alpha_i} = 0. \tag{3.5}$$

So,

$$\omega = \sum_{i=1}^{N} \alpha_i \phi(x_i), \qquad \sum_{i=1}^{N} \alpha_i = 0, \quad \alpha_i = \eta e_i, \omega^T \phi(x_i) + b + e_i - y_i = 0, \ i = 1, 2, \ldots, N. \tag{3.6}$$

The solution of (3.6), α_i and b, can be computed from the input of the sample sets when the LS-SVM is trained. Applying the Mercer condition one obtains [22]:

$$K(x_k, x_l) = \varphi(x_k)^T \varphi(x_l), \quad k, l = 1, 2, \ldots, N. \tag{3.7}$$

Thus, the LS-SVM model for nonlinear estimation is illustrated as (3.8).

$$y(x) = \sum_{i=1}^{N} \alpha_i K(x, x_i) + b. \tag{3.8}$$

The RBF kernel is used as the kernel function of the LS-SVM in this paper:

$$K(x, x_i) = \exp\left(-\frac{\|x - x_i\|^2}{2\sigma^2}\right). \tag{3.9}$$

As mentioned above, regularisation parameter (η) and kernel width (σ) need to be selected. In order for an optimal combination determined before the LS-SVM is trained, we use a simplified cross-validation method developed by Xu et al. [22], which defines a training set, consisting of the validation subsets and the verification subsets. Validation subset is used to train LS-SVM with some empirical combinations of tuning parameters. The primary parameters are those combinations which make the output of the LS-SVM approach the given accuracy. On the other hand, verification set is used to further train LS-SVM. As a result, the final selection of tuning parameters is made, and the system model is also obtained.

3.2. The Input/Output Design of LS-SVM

Due to the position and velocity changes with time, there is an HF states variation. It has been found that there is a correlation between states measured by INS and the HF states. Although modeling this correlation is difficult, it is able to build correlation with designed LS-SVM after adequate training. When the signals in WSNs are unavailable, with the input of INS's own estimation error of position and velocity, the LS-SVM is able to output the correction value for position and velocity, respectively, which is used to compensate the INS solution (as the integration HF does when the signals in WSN are available). As mentioned above, the
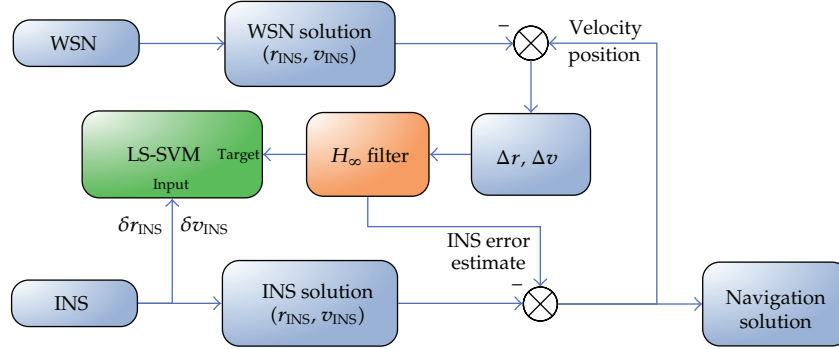
Figure 1: Configuration of the LS-SVM/HF hybrid system.

estimation errors of position and velocity measured by INS are selected as the input of the LS-SVM, which is illustrated as (3.10):

$$\text{LS-SVM}_{\text{in}} = \{\delta r_x, \delta r_y, \delta v_x, \delta v_y\}. \tag{3.10}$$

And the output of the LS-SVM can be simplified as:

$$\text{LS-SVM}_{\text{out}} = \{\Delta r_x, \Delta r_y, \Delta v_x, \Delta v_y\}. \tag{3.11}$$

The structure of LS-SVM is consistently implemented for the training and prediction stages.

4. LS-SVM and HF Hybrid Method for Integration System

In this section, the LS-SVM/HF architecture is designed. The integration navigation consists of two stages. One is the LS-SVM/HF hybrid system. The other is the LS-SVM-based prediction during WSN outages.

4.1. The LS-SVM/HF Hybrid System for INS/WSN

The LS-SVM is in the training mode when the signals in WSNs are available. Figure 1 displays the configuration of the integration system for training of LS-SVM. INS estimates the errors of position and velocity in two directions which are continuously input to the LS-SVM for training. Meanwhile, the output of HF is employed for the target vectors of the training. The differences of position ($r_{\text{WSN}}, r_{\text{INS}}$) and velocity ($v_{\text{WSN}}, v_{\text{INS}}$) between INS and WSN are used for the observation vectors of the HF.

4.2. The Configuration of the LS-SVM-Based Prediction during WSN Outages.

The integrated system becomes a stand-alone INS without WSN signal. The LS-SVM is in the prediction mode now, and the output of the LS-SVM is used for error compensation.
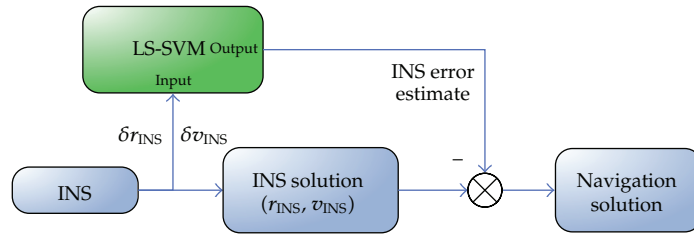
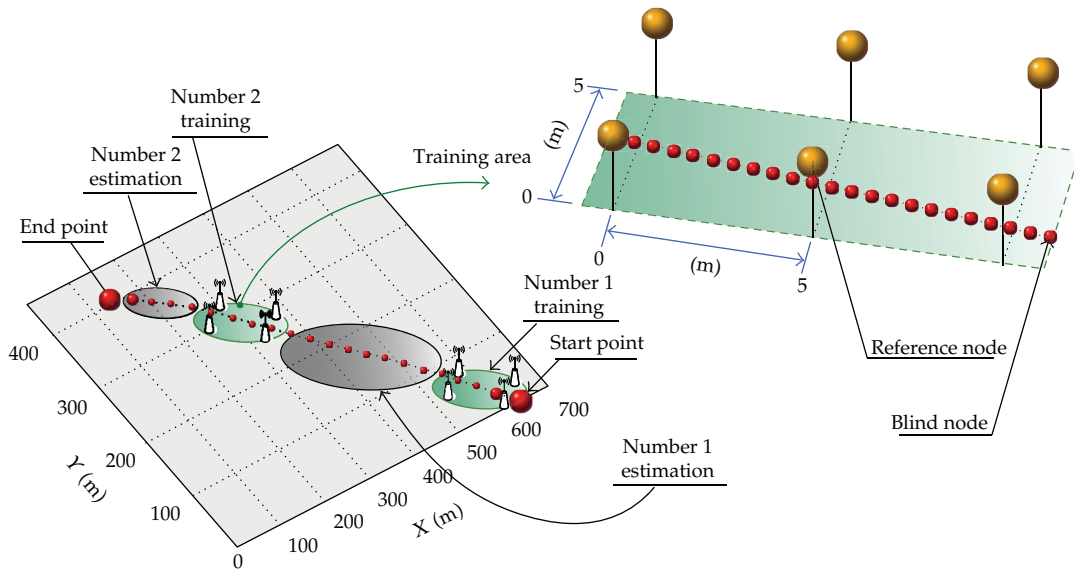**Figure 2:** Configuration of the LS-SVM-based prediction during WSN outages.

Figure 3: Definition of simulation scenarios.

The errors of position and velocity estimated by INS are continuously input to the LS-SVM as it was done during the training stage. The configuration of the LS-SVM-based prediction during WSN outage is illustrated in Figure 2.

5. Simulation and Performance

5.1. Assumptions

In order to assess the performance of the proposed method, the simulation is implemented. A 700 m × 450 m area is defined as simulation scenario. In simulation, we assume that a BN moves from start point (650, 0) to end point (130, 400) along the red-dotted line in Figure 3. Based on the real-time data measured by INS, two areas (denote as green) is set as training area, where the signals in WSN are available. The scale of one training area is about 150 m × 150 m (denote as no.1 training area), and the other one is about 100 m × 100 m (denote as no.2 training area). The range between RNs is 5 m, and the communication range is 11 m. The sampling period (T) in (2.3) is set to 1s. Here, we assume that the WSNs employ ultrasonic waves for localization, which is similar to [13], and the accuracy of localization is about 20 cm.

Table 1: LS-SVM training results with the validation set.

No.	σ	η	Errors with validation set					
			$\delta(\delta r_x)$ (m)	$\delta(\delta r_y)$ (m)	Mean error (m)	$\delta(\delta v_x)$ (m/s)	$\delta(\delta v_y)$ (m/s)	Mean error (m/s)
1	1	1	0.5991	0.2046	0.3558	0.1338	0.0864	0.1101
2	1	100	0.2354	0.1126	0.1711	0.0913	0.0968	0.0941
3	1	1000	0.2331	0.1067	0.1699	0.0932	0.0959	0.0946
4	30	100	0.2862	0.1067	0.1967	0.0924	0.0914	0.0919
5	30	1000	0.2542	0.1071	0.1807	0.0921	0.0926	0.0924
6	50	100	0.2871	0.1071	0.1972	0.0922	0.0912	0.0917
7	50	1000	0.2610	0.1073	0.1839	0.0918	0.0924	0.0921
8	100	100	0.2933	0.1068	0.2009	0.0923	0.0903	0.0913
9	100	1000	0.2641	0.1085	0.1852	0.0915	0.0923	0.0919
10	1000	1000	0.2903	0.1063	0.1452	0.0922	0.0900	0.0911

5.2. LS-SVM Training

In this paper, we define an independent training set with 100 points, the first 50 points are the validation subset, and other points are the verification subset. LS-SVM training results with the validation set are listed in Table 1. From Table 1, the final selection of tuning parameters is $\sigma = 1000$ and $\eta = 1000$. Finally, using both the validation and verification sets as well as the selected tuning parameters, the LS-SVM was trained again to obtain the compensation model.

5.3. Performance Analysis

According to Theorem 2.3, we readily obtain the following parameters for HF which is used in training area.

To the HF used in the first training area,

$$
E = \begin{bmatrix} 0 & 0 & -0.0012 & 0 \\ 0 & 0 & 0 & -0.0012 \\ 0 & 0 & 0 & 0 \\ 0 & 0 & 0 & 0 \end{bmatrix}, \qquad \gamma = 4.0055,
$$

$$(5.1)$$

$$
A_f = e^{-11} \begin{bmatrix} -0.0044 & -0.0694 & 0.0658 & 0.0082 \\ 0.0066 & -0.0146 & -0.0296 & 0.0379 \\ -0.0588 & 0.1083 & -0.0353 & -0.0142 \\ 0.0553 & -0.0232 & -0.0009 & -0.0316 \end{bmatrix}, \qquad B_f = \begin{bmatrix} 1 & 0 & 0.2 & 0 \\ 0 & 1 & 0 & 0.2 \\ 0 & 0 & 1 & 0 \\ 0 & 0 & 0 & 1 \end{bmatrix}.
$$

Table 2: The mean errors of position and velocity for the INS-only, KF, and HF methods in the training area.

Mode	$\delta(\delta r_x)$ (m)		$\delta(\delta r_y)$ (m)		$\delta(\delta v_x)$ (m/s)		$\delta(\delta v_y)$ (m/s)	
	No. 1 area	No. 2 area	No. 1 area	No. 2 area	No. 1 area	No. 2 area	No. 1 area	No. 2 area
INS-only	7.8315	40.6179	4.7923	36.0891	0.6584	2.0649	1.5777	2.0649
KF	2.9170	14.9663	1.7916	13.2591	0.2715	0.3155	0.5984	0.8856
HF	0.3881	0.4958	0.5338	0.8464	0.1064	0.1041	0.1008	0.0932

To the HF used in the second training area,

$$E = e^{-3} \begin{bmatrix} 0 & 0 & 0.8409 & 0 \\ 0 & 0 & 0 & 0.8409 \\ 0 & 0 & 0 & 0 \\ 0 & 0 & 0 & 0 \end{bmatrix}, \quad \gamma = 4.0055,$$

$$A_f = e^{-11} \begin{bmatrix} 0.0857 & -0.0230 & -0.0524 & -0.0106 \\ -0.0087 & -0.0476 & 0.0416 & 0.0153 \\ -0.0626 & 0.1602 & -0.0407 & -0.0571 \\ -0.0153 & -0.0912 & 0.0568 & 0.0495 \end{bmatrix}, \quad B_f = \begin{bmatrix} 1 & 0 & 0.21 & 0 \\ 0 & 1 & 0 & 0.21 \\ 0 & 0 & 1 & 0 \\ 0 & 0 & 0 & 1 \end{bmatrix}. \tag{5.2}$$

Figures 4 and 5 display the position errors in x-direction and y-direction in the first training area. The HF result is compared with the INS-only solution and the KF solution. In those figures one can see that both the KF and HF can reduce the position errors in x direction and y direction, respectively, and that the HF solution has the smallest error. Simulation result shows that the proposed HF method is very effective as it decreases the mean errors of position by about 85% in x direction and by about 80% in y direction compared with KF.

To further clearly demonstrate how the proposed HF improves the accuracy of the solution, the velocity errors in x-direction and y-direction for the INS-only, KF, and HF methods are shown in Figures 6 and 7. Note that the errors for the HF are smaller than the ones for the KF and INS-only methods both in x direction and y direction, confirming that the proposed algorithm can improve system performance. Simulation result shows that the proposed HF method decreases the velocity errors by about 70% in x direction and in y direction errors by about 75% compared with KF.

The mean errors of position and velocity in x direction and y direction in the second training area are illustrated in Table 2. We can see that the improvement is also particularly obvious.

In order to assess the performance of the hybrid method, two WSN outages are simulated. The LS-SVM result is compared with the INS-only solution and the BP solution during these outages. The position errors in x direction and y direction after the first training area derived from the INS-only (in green), BP (in blue), and the LS-SVM (in red) methods are shown in Figures 8 and 9, respectively. The BP method has the same input/output as the LS-SVM. In Figures 8 and 9, one can see that both the BP and LS-SVM are able to reduce the position errors, and that the HF solution has the smallest error, confirming that the proposed algorithm can improve system performance. From these outage results it can be seen that
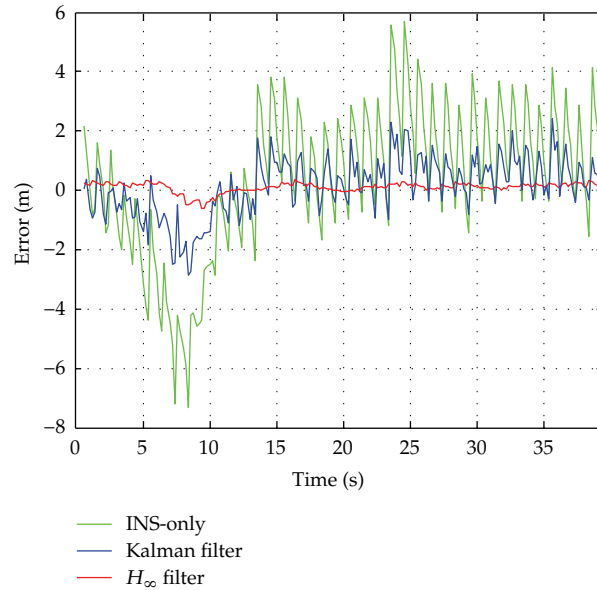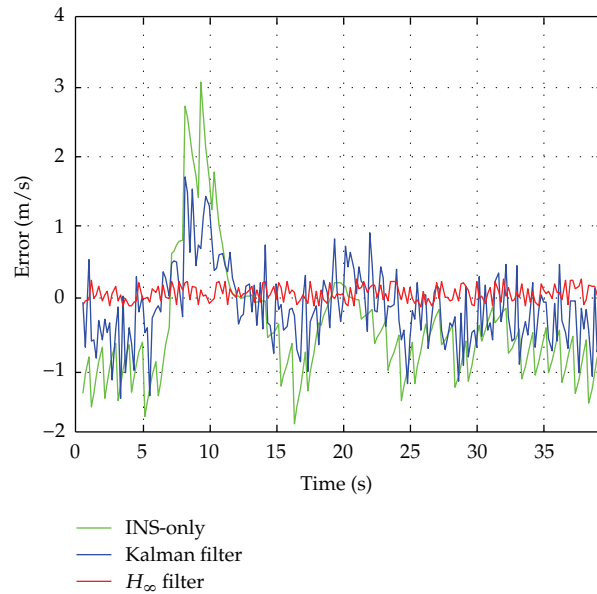
Figure 4: The position errors in x direction for the INS-only, KF, and HF methods in the first training area.
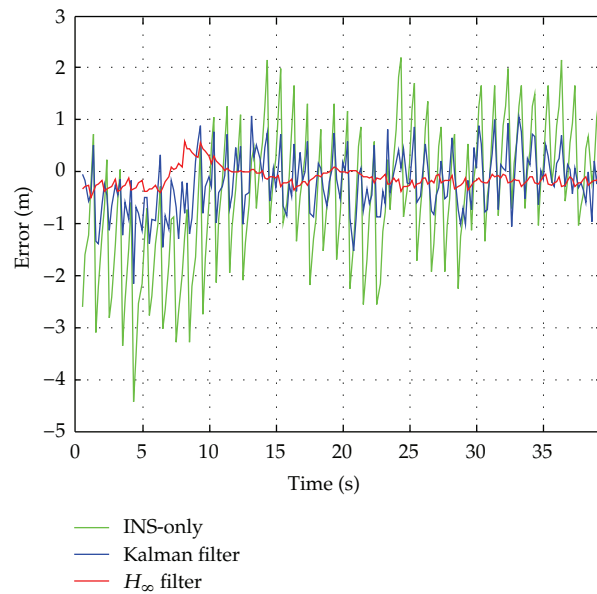
Figure 5: The position errors in y direction for the INS-only, KF, and HF methods in the first training area.

the proposed method decreases by about 80% position errors in x direction and 70% position errors in y direction compared with BP.

Figures 10 and 11 display the velocity errors in x-direction and y-direction in the first 50-second WSN outages area. The LS-SVM results are compared with the INS-only solution and the BP solution. In those figures one can see that both the LS-SVM and BP can reduce

Figure 6: The velocity errors in x direction for the INS-only, KF, and HF methods in the first training area.
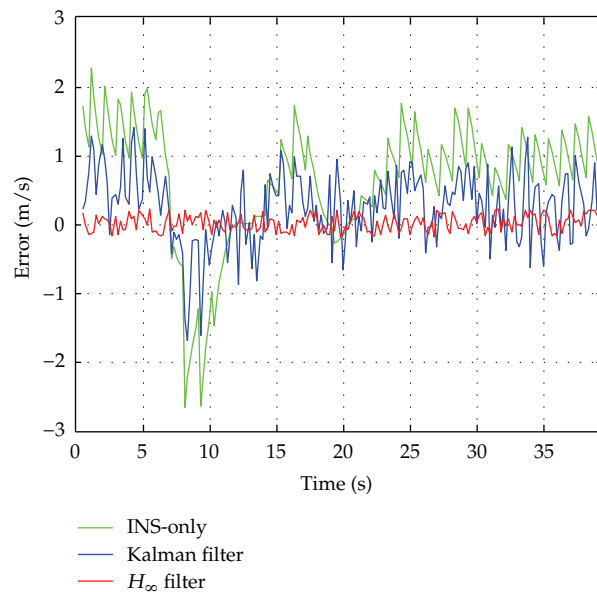

Figure 7: The velocity errors in y direction for the INS-only, KF, and HF methods in the first training area.

the position errors, and that the LS-SVM solution has the smallest error. However, there are some fluctuations in BP's error. The mean errors of position and velocity in x direction and y direction in the second WSN outages area are illustrated in Table 3. Simulation result shows that the proposed LS-SVM method is very effective as it decreases the mean errors of velocity by about 40% in x direction and by about 70% in y direction compared with BP.
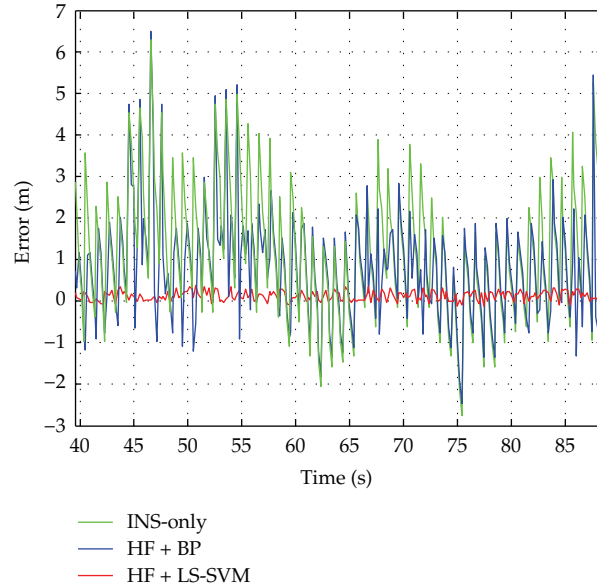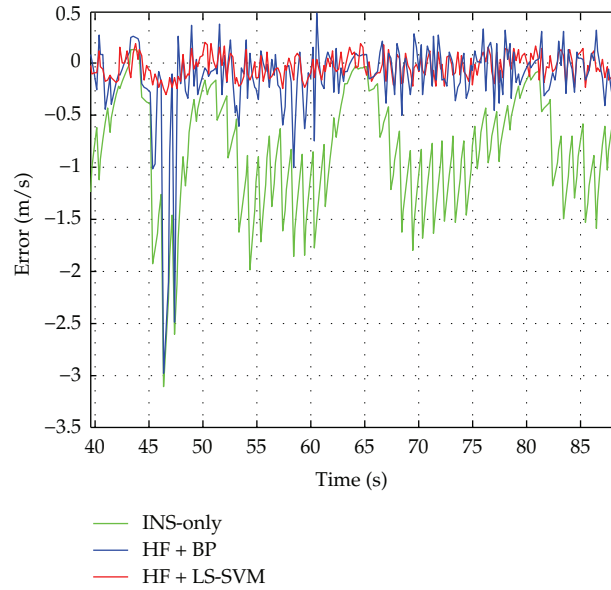
Figure 8: The position errors in x direction for the INS-only, HF + BP, and HF + LS-SVM methods in the first WSN outages.
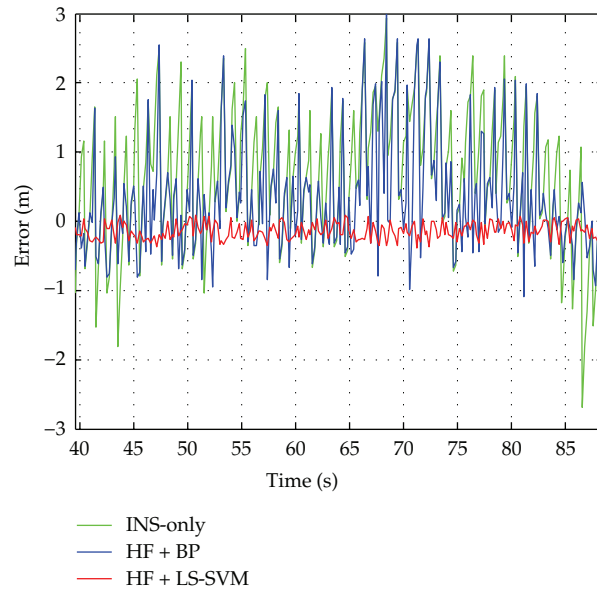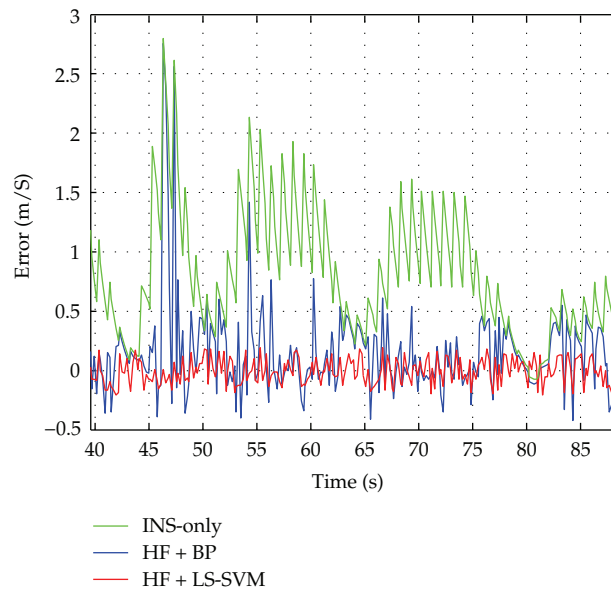

Figure 9: The position errors in y direction for the INS-only, HF + BP, and HF + LS-SVM methods in the first WSN outages.

As mentioned above, the improvement is particularly obvious in the prediction period. The prediction of the LS-SVM is able to maintain a higher accuracy and reduce the influence of accuracy deterioration caused by the INS.

Figure 10: The velocity errors in x direction for the INS-only, HF + BP, and HF + LS-SVM methods in the first WSN outages.

Figure 11: The velocity errors in y direction for the INS-only, HF + BP, and HF + LS-SVM methods in the first WSN outages.

6. Conclusions

This work proposes an integrated INS/WSN system using LS-SVM and HF. The input and output of an LS-SVM are selected on the basis of correlations between the estimation errors measured by INS and the HF states. When the signals in WSN are available, the HF

Table 3: The mean errors of position and velocity for the INS-only, KF, and HF methods in the prediction area.

Mode	$\delta(\delta r_x)$ (m)		$\delta(\delta r_y)$ (m)		$\delta(\delta v_x)$ (m/s)		$\delta(\delta v_y)$ (m/s)	
	No. 1 area	No. 2 area	No. 1 area	No. 2 area	No. 1 area	No. 2 area	No. 1 area	No. 2 area
INS-only	12.1524	72.4795	8.7879	70.0089	0.8897	3.0793	2.0265	6.0012
BP	5.2628	36.4784	4.9441	36.5174	0.6502	1.1008	0.8096	1.6045
LS-SVM	0.5916	5.2938	0.4676	4.6548	0.0786	0.0092	0.0754	0.0567

is employed to provide optimal estimation of position and velocity errors, which is used to update the INS solution. Meanwhile, mapping model between the estimation errors of INS and the HF states is trained by the LS-SVM. Based on the real-time data measured by INS, WSNs enabled and outages areas are simulated. The results show an improved overall performance in comparison with the results of the INS-only and KF solutions, and the prediction of the LS-SVM has a higher accuracy than the prediction of the BP.
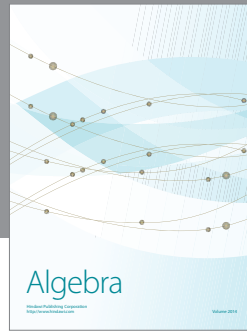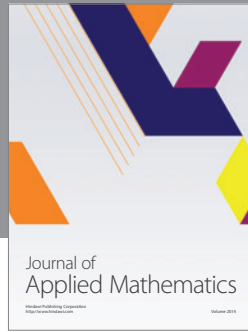
Acknowledgments

References

[1] G. Retscher and Q. Fu, "An intelligent personal navigator integrating GNSS, RFID and INS for continuous position determination," *Boletim de Ciências Geodésicas*, vol. 15, no. 5, pp. 707–724, 2009.

[2] S. H. Fang and T. N. Lin, "Cooperative multi-radio localization in heterogeneous wireless networks," *IEEE Transactions on Wireless Communications*, vol. 9, no. 5, Article ID 5463208, pp. 1547–1551, 2010.

[3] J. Caffery Jr. and G. L. Stüber, "Subscriber location in CDNA cellular networks," *IEEE Transactions on Vehicular Technology*, vol. 47, no. 2, pp. 406–416, 1998.

[4] H. Liu, H. Darabi, P. Banerjee, and J. Liu, "Survey of wireless indoor positioning techniques and systems," *IEEE Transactions on Systems, Man and Cybernetics Part C*, vol. 37, no. 6, pp. 1067–1080, 2007.

[5] Y. Zhao, "Standardization of mobile phone positioning for 3G systems," *IEEE Communications Magazine*, vol. 40, no. 7, pp. 108–116, 2002.

[6] M. Vossiek, L. Wiebking, P. Gulden, J. Wieghardt, C. Hoffmann, and P. Heide, "Wireless local positioning," *IEEE Microwave Magazine*, vol. 4, no. 4, pp. 77–86, 2003.

[7] Y. K. Huang, A. C. Pang, and H. N. Hung, "A comprehensive analysis of low-power operation for beacon-enabled IEEE 802.15.4 wireless networks," *IEEE Transactions on Wireless Communications*, vol. 8, no. 11, Article ID 5336787, pp. 5601–5611, 2009.

[8] R. W. Ouyang, A. K. S. Wong, and C. T. Lea, "Received signal strength-based wireless localization via semidefinite programming: noncooperative and cooperative schemes," *IEEE Transactions on Vehicular Technology*, vol. 59, no. 3, Article ID 5378537, pp. 1307–1318, 2010.

[9] N. Patwari, A. O. Hero III, M. Perkins, N. S. Correal, and R. J. O'Dea, "Relative location estimation in wireless sensor networks," *IEEE Transactions on Signal Processing*, vol. 51, no. 8, pp. 2137–2148, 2003.

[10] S. Al-Jazzar and J. Caffery Jr., "ML & Bayesian TOA location estimators for NLOS environments," in *Proceedings of the 56th IEEE Vehicular Technology Conference*, vol. 2, pp. 1178–1181, September 2002.

[11] S. Al-Jazzar, M. Ghogho, and D. McLernon, "A joint TOA/AOA constrained minimization method for locating wireless devices in non-line-of-sight environment," *IEEE Transactions on Vehicular Technology*, vol. 58, no. 1, pp. 468–472, 2009.

[12] N. A. Alsindi, B. Alavi, and K. Pahlavan, "Measurement and modeling of ultrawideband TOA-based ranging in indoor multipath environments," *IEEE Transactions on Vehicular Technology*, vol. 58, no. 3, pp. 1046–1058, 2009.

[13] M. Minami, H. Morikawa, and T. Aoyama, "Design and implementation of a fully distributed ultrasonic positioning system," *Electronics and Communications in Japan, Part III*, vol. 90, no. 6, pp. 17–26, 2007.

[14] J. Lobo, P. Lucas, J. Dias, and A. T. de Almeida, "Inertia navigation system for mobile land vehicles," in *Proceedings of the IEEE International Symposium on Industrial Electronics (ISIE '95)*, vol. 2, pp. 843–848, July 1995.

[15] X. Chen, J. Yu, and M. Gu, "Study on tightly-coupled GPS/SINS integrated navigation system by using software GPS receiver," in *Proceedings of the 12th IEEE Instrumentation and Measurement Technology Conference (MTC '11)*, pp. 1062–1065, May 2011.

[16] D. K. Mynbaev, "Errors of an inertial navigation unit caused by ring laser gyros errors (PLANS '94)," in *Proceedings of the IEEE Position Location and Navigation Symposium*, pp. 833–838, Las Vegas, Nev, USA, April 1994.

[17] A. Noureldin, D. Irvine-Halliday, and M. P. Mintchev, "Accuracy limitations of FOG-based continuous measurement-while-drilling surveying instruments for horizontal wells," *IEEE Transactions on Instrumentation and Measurement*, vol. 51, no. 6, pp. 1177–1190, 2002.

[18] J. Kim, J. Lyou, and H. Kwak, "Vision coupled GPS/INS scheme for helicopter navigation," *Journal of Mechanical Science and Technology*, vol. 24, no. 2, pp. 489–496, 2010.

[19] F. Berefelt, B. Boberg, J. Nygårds, P. Strömbäck, and S. L. Wirkander, "Collaborative GPS/INS navigation in urban environment," in *Proceedings of the Institute of Navigation National Meeting (NTM '04)*, pp. 1114–1125, San Diego, Calif, USA, January 2004.

[20] A. El-Rabbany and M. El-Diasty, "An efficient neural network model for de-noising of MEMS-based inertial data," *Journal of Navigation*, vol. 57, no. 3, pp. 407–415, 2004.

[21] J. J. Wang, J. Wang, D. Sinclair, and L. Watts, "A neural network and Kalman filter hybrid approach for GPS/INS integration," in *Proceedings of the 12th International Association of Institutes of Navigation (IAIN) World Congress & 2006 International Symposium on GPS/GNSS*, pp. 277–282, Jeju, Korea, 2006.

[22] Z. Xu, Y. Li, C. Rizos, and X. Xu, "Novel hybrid of LS-SVM and kalman filter for GPS/INS integration," *Journal of Navigation*, vol. 63, no. 2, pp. 289–299, 2010.

[23] F. Chen and M. W. Dunnigan, "Comparative study of a sliding-mode observer and Kalman filters for full state estimation in an induction machine," *IEE Proceedings: Electric Power Applications*, vol. 149, no. 1, pp. 53–64, 2002.

[24] E. Wan and R. Merwe, "The unscented Kalman filter for nonlinear estimation," in *Proceedings of the Adaptive Systems for Signal Processing, Communications, and Control Symposium (AS-SPCC '00)*, pp. 153–158, Alberta, Canada, October 2000.

[25] B. S. Chen and W. Zhang, "Stochastic H_2/H_∞ control with state-dependent noise," *IEEE Transactions on Automatic Control*, vol. 49, no. 1, pp. 45–57, 2004.

[26] W. Zhang, H. Zhang, and B. S. Chen, "Stochastic H_2 / H_∞ control with (x, u, v)-dependent noise: finite horizon case," *Automatica*, vol. 42, no. 11, pp. 1891–1898, 2006.

[27] W. Zhang and L. Xie, "Interval stability and stabilization of linear stochastic systems," *IEEE Transactions on Automatic Control*, vol. 54, no. 4, pp. 810–815, 2009.

[28] W. Zhang, B. S. Chen, and C. S. Tseng, "Robust H_∞ filtering for nonlinear stochastic systems," *IEEE Transactions on Signal Processing*, vol. 53, no. 2, pp. 589–598, 2005.

[29] W. Zhang and B. S. Chen, "On stabilizability and exact observability of stochastic systems with their applications," *Automatica*, vol. 40, no. 1, pp. 87–94, 2004.

[30] S. Xu and T. Chen, "Robust H_∞ filtering for uncertain impulsive stochastic systems under sampled measurements," *Automatica*, vol. 39, no. 3, pp. 509–516, 2003.

[31] E. Gershon, U. Shaked, and I. Yaesh, "Robust H_∞ estimation of stationary discrete-time linear processes with stochastic uncertainties," *Systems and Control Letters*, vol. 45, no. 4, pp. 257–269, 2002.